Crystal Structure of a Trapped Phosphate Intermediate in Vanadium Apochloroperoxidase Catalyzing a Dephosphorylation Reaction‡

Sandra de Macedo-Ribeiro,§,|| Rokus Renirie,⊥ Ron Wever,⊥ and Albrecht Messerschmidt*,§

Abteilung Proteomics und Signaltransduktion, Max-Planck-Institut für Biochemie, Am Klopferspitz 18, 82152 Martinsried, Germany, and Van't Hoff Institute of Molecular Sciences, University of Amsterdam, 1018 WS Amsterdam, The Netherlands

Received September 12, 2007; Revised Manuscript Received November 14, 2007

ABSTRACT: The crystal structure of the apo form of vanadium chloroperoxidase from *Curvularia inaequalis* reacted with para-nitrophenylphosphate was determined at a resolution of 1.5 Å. The aim of this study was to solve structural details of the dephosphorylation reaction catalyzed by this enzyme. Since the chloroperoxidase is functionally and evolutionary related to several acid phosphatases including human glucose-6-phosphatase and a group of membrane-bound lipid phosphatases, the structure sheds light on the details of the dephosphorylation catalyzed by these enzymes as well. The trapped intermediate found is bound to the active site as a metaphosphate anion PO_3^-, with its phosphorus atom covalently attached to the $N^{\epsilon 2}$ atom of His496. An apical water molecule is within hydrogen-bonding distance to the phosphorus atom of the metaphosphate, and it is in a perfect position for a nucleophilic attack on the metaphosphate−histidine intermediate to form the inorganic phosphate. This is, to our knowledge, the first structural characterization of a real reaction intermediate of the inorganic phosphate group release in a dephosphorylation reaction.

Vanadium haloperoxidases are enzymes that catalyze the oxidation of halides to their corresponding hypohalous acids at the expense of hydrogen peroxide

$$H_2O_2 + H^+ + X^- \rightarrow H_2O + HOX \qquad (1)$$

Haloperoxidases are named after the most electronegative halide they are able to oxidize; thus, a chloroperoxidase oxidizes Cl^-, Br^-, and I^-. If a convenient nucleophilic acceptor is present, a reaction will occur with HOX to form a diversity of halogenated reaction products. Many of these organohalogens have biocidal effects, and this may provide defense functions.

The crystal structure of the first vanadium haloperoxidase, the chloroperoxidase (VCPO)[1] from the fungus *Curvularia inaequalis*, and the proposal of a mechanism based on the structure, mutation studies, and functional analyses allowed a further understanding of the chemistry of vanadium in this system (*1*−*5*). VCPO is related to vanadium bromoperoxidases (VBPOs) from the brown seaweed *Ascophyllum nodosum* and the red algae *Corallina* species, whose crystal structures have also been solved (*6*, *7*). The VBPOs show a similar mainly α-helical fold of the monomers, but they share only a common four-helix bundle with VCPO. The amino acid (aa) residue stretch spanning the four-helix bundle and the subsequent C-terminal loop contains all residues forming the active site that binds the vanadium in the form of vanadate (HVO_4^{2-}) as the prosthetic group. The structures of the actives site of all vanadium haloperoxidases align very well. The vanadium is coordinated to His496 (VCPO numbering throughout if not otherwise stated), and the residues Lys353, Arg360, Ser402, Gly403, and Arg490 form hydrogen bonds with the non-protein oxygens of vanadate. His404 was proposed to function as the acid−base group in catalysis. The main difference between VCPOs and VBPOs is the substitution of Phe397 to His (411 in VBPO from *A. nodosum*).

An aa sequence database search revealed an unexpected homology between the vanadium haloperoxidases and three families of acid phosphatases, indicating similarities in the anion binding active sites of all these enzymes including human glucose-6-phosphatase (*8*−*10*) and lipid phosphate hydrolases (*11*). Together with the similar structural and chemical features of vanadate and phosphate, this prompted a study to check the possible phosphatase activity of vanadium haloperoxidases. Indeed, the recombinant apo-VCPO using para-nitrophenylphosphate (pNPP) as a substrate showed phosphatase activity (*8*). Similarly, acid phosphatase substituted with vanadate in the active site showed haloperoxidase activity (*12*).

The crystal structures of the acid phosphatases from *Escherichia blattae* (EB-AP) and *Salmonella typhimurium* (PhoN), members of the family related to the haloperoxidases, were determined both in the native form with sulfate

‡ Coordinates of the structure described in this paper have been deposited in the Protein Data Bank with ID 3BB0.

* Corresponding author. Tel.: +49 89 8578 2669; fax: +49 89 8578 2219; e-mail: messersc@biochem.mpg.de.

§ Max-Planck-Institut für Biochemie.

|| Current address: Instituto de Biologia Molecular e Celular, Rua do Campo Alegre 823, 4150-180 Porto, Portugal.

⊥ University of Amsterdam.

[1] Abbreviations: VCPO, vanadium chloroperoxidase from *Curvularia inaequalis*; VBPO, vanadium bromoperoxidase; pNPP, para-nitrophenylphosphate; EB-AP, acid phosphatase from *Escherichia blattae*; PhoN, acid phosphatase from *Salmonella typhimurium*; apo-VCPO-pNPP, apo-VCPO reacted with para-nitrophenylphosphate; K_d, dissociation constant; aa, amino acid; rmsd, root mean square deviation; ESU, estimated standard uncertainty.

10.1021/bi7018628 CCC: $40.75
Published on Web 12/29/2007

bound to the active site and in complex with the transition-state analogue molybdate (*13*) or tungstate and phosphate, respectively (*14*). The comparison of the crystal structures of EB-AP, PhoN, and VCPO reveals a striking similarity in the active site structures. In addition, the topology of the EB-AP and PhoN cores shows considerable similarity to the fold of the active site containing part of the vanadium dependent haloperoxidases despite the lack of further aa sequence identity. This definitely confirmed the conclusions drawn from the aa sequence database search. A structural and functional comparison between the relevant acid phosphatase enzymes and the other vanadium haloperoxidases was performed with a corroboration of the earlier results (*15*).

The phosphatase activity of active site mutants of VCPO from *C. inaequalis* has been determined, and a proposal of the mechanism for the hydrolysis of a phosphate monoester by apo-VCPO has been made (*5*). The low phosphatase activity (1.2 min^{-1}) as compared to normal phosphatases (*5*) allowed pre-steady-state studies on both native enzyme and mutants. These data suggested the existence of a phospho−enzyme intermediate whose breakdown is rate limiting. In the mechanism proposed, the histidine that binds to the vanadate cofactor in holo-VCPO acts as a nucleophile forming a phosphoryl intermediate. Recently, a structural and mutational analysis of the PhoN phosphatase was reported (*14*), indeed confirming the role of His197 in PhoN in the formation of a phosphohistidine intermediate. Here, we report the crystal structure of recombinant apo-VCPO reacted with pNPP, which shows a trapped phosphohistidine intermediate that is formed as a result of the reaction in the active site.

EXPERIMENTAL PROCEDURES

Crystallization and Data Collection. Recombinant apo-VCPO was overexpressed in *Saccharomyces cerevisiae* and purified as described previously (*1*). Crystals grew at 4 °C by vapor diffusion. Hanging drops were made from 3 μL of protein solution (5 mg mL^{-1} in 5 mM MOPS, pH 7.5) and 3 μL of precipitating buffer containing 1.7 M ammonium sulfate, 0.1 M Tris-HCl, pH 8.0, and 0.3 μL of 10 mM cysteine-HCl. The crystals belong to space group *R*3 and are isomorphous to the crystals from the native protein. The recombinant material tends to form crystalline precipitates when the crystallization conditions used to grow the native crystals are used. Thus, the crystallization conditions were altered to allow for slower equilibration rates. The crystals from the recombinant material take 2−3 months to grow. For the preparation of the apo-VCPO-pNPP intermediate complex, apo-VCPO crystals were soaked for 10 min in a solution containing 1 mM pNPP, 2.6 M ammonium sulfate, and 0.15 M Tris-H_2SO_4 at pH 8.0.

Cryo data were collected from a flash-cooled apo-VCPO-pNPP crystal (30.0% glycerol, 2.6 M ammonium sulfate, 0.15 M Tris-HCl, pH 8.0) on the wiggler beamline BW6 at DORIS (DESY, Hamburg, Germany). Data were processed with MOSFLM (*16*) and programs from the CCP4 suite (*17*). Crystal parameters and data collection statistics are depicted in Table 1.

Structure Determination and Crystallographic Refinement. The crystallographic phases of the native form (*4*) were used as the starting phases for the refinement of the apo-VCPO-pNPP form of the enzyme. The model was refined with REFMAC5 (*18*). The equilibrium bond lengths and angles for the restraining of the metaphosphate anion PO_3^- were taken from Range et al. (*19*). Thereby, the molecule is planar with P═O bonds with formal bond orders of 5/3 and equal bond distances of 1.509 Å. The P−N distance between the PO_3^- group and the $N^{\epsilon 2}$ atom of His496 was not restrained during the refinement. The crystallographic refinement converged, giving satisfactory *R*-factors. The detailed refinement statistics for the final model are listed in Table 1. The stereochemistry of the model was analyzed with PROCHECK (*20*).

Table 1: Data Collection and Refinement Statistics of Apo-VCPO-pNPP Derivative

Data collection[a]	
wavelength (Å)	1.05
space group	*R*3
resolution range (Å)	50.0−1.50 (1.53−1.50)
unit cell params (Å)	$a = b = 128.06$, $c = 103.31$
Diffraction data	
no. of unique observations	100278 (5046)
redundancy	1.8
$I/\sigma(I)$	8.2 (3.5)
completeness (%)	99.1 (96.0)
R_{merge}[b] (%)	6.2 (31.7)
Refinement[a]	
resolution range (Å)	14.9−1.50 (1.54−1.50)
R_{factor}[c] (%)	17.4 (19.7)
R_{free} (%), test set 5.1%	19.4 (23.5)
rmsd bond lengths (Å)	0.009
rmsd bond angles (deg)	1.2
total no. of atoms	5308
av *B*-factor (protein, Å^2)	15.6
av *B*-factor (water, Å^2)	30.5
rmsd for bonded B[d] (Å^2)	1.1
ESU based on R_{factor} (Å)	0.071
ESU based on R_{free} (Å)	0.070
ESU based on maximum likelihood (Å)	0.041

[a] Numbers in parentheses represent data for the highest resolution shell (as given). [b] $R_{merge} = \sum(I - \langle I \rangle)/\sum I$. [c] $R_{factor} = \sum(|F_{obsd}| - |F_{calcd}|)/\sum|F_{obsd}|$. [d] rmsd of bonded *B*-factors: a measure of smoothness of the *B*-factor refinement.

In the structure, residues 1−3 and 580−609 were excluded from the model because they were not visible in the electron density and are probably mobile or disordered. Residues 118−127 are poorly defined in the electron density reflected by high temperature factors. Residues 390−395 exhibit an electron density of medium quality, indicating a higher flexibility of this structural part. Cys69 shows electron density for an additional oxygen atom and has been modeled as *S*-hydroxycysteine. The appearance of the side chain of residue 544 was that of an arginine instead of a proline as given in the deduced amino acid sequence for this expression construct. Therefore, it was modeled as arginine. The relevant region in the difference electron density shows no positive and negative residual density, proving that this replacement is correct with a high degree of probability.

For the superimpositions of structures, the program LSQMAN (*21*) was used. Figures of the protein structure were prepared with PyMol (*22*). The coordinates and structure factors have been submitted to the Protein Data Bank with PDB ID 3BB0.

RESULTS AND DISCUSSION

Overall Structure. Superpositions of the refined protein model with the native enzyme (1VNC (*4*)) and the recom-

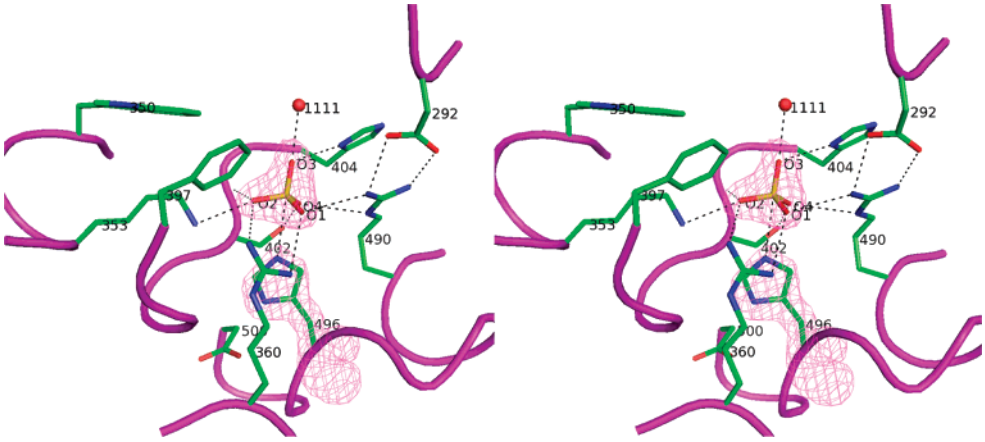

FIGURE 1: Stereoview of the hydrogen-bonding pattern around the active site of apo-VCPO. The sulfate is displayed with oxygens in red and the sulfur atom in yellow. The hydrogen bonds and other relevant interactions with the sulfate ion are represented as dashed lines, and the distances are given in Table 2. The electron density map contoured at 4.0σ was calculated after omitting His496 and the bound sulfate ion.

binant apoenzyme (1VNS (*2*)) revealed that the overall backbone structure remains unchanged with rmsds of the atomic coordinates of the C_α atoms of 0.21 Å between apo-VCPO-pNPP and 1VNC and 0.24 Å between VCPO-pNPP and 1VNC. The residues in the active site are clearly defined in the electron density map. The region of residues Asp390 to Pro396 is a part of the hydrophobic side from the broad channel, which leads to the active site and adopts a different conformation in the recombinant Asp292Ala mutant (*2*). Here, its conformation has not been changed as compared to the structures of the native enzyme (1VCN) and the recombinant apo form (1VNS). Residues 390−395 are very flexible in the recombinant protein material, although their density was clearly defined in the native protein model. The same is true for the protein segment including residues 200−220. The amino acid residues included in these regions are the same as in the native enzyme, and the nucleotide sequence in this region has been reconfirmed. Thus, the alterations in the conformations of these residues could be a consequence of misfolding of the protein in the *S. cerevisiae* expression system. As a result, the protein expressed recombinantly is more difficult to crystallize, and the crystals obtained have one or the other predominant conformation.

The identification of an arginine in position 544 in the electron density map in place of a proline may be explained by a sequencing error. The amino acid sequence of VCPO from *C. inaequalis* was determined by cDNA sequencing techniques (*23*). The codon change from Pro to Arg needs one nucleotide exchange only, which appears to be very likely. It is also conceivable that this particular codon is incorrectly read by the RNA polymerase. This amino acid sequence conflict has been apparent in all X-ray structures both of natural VCPO (PDB ID 1VNC) and recombinant VCPO expressed in yeast (PDB ID 1VNS). In these X-ray structures, the respective residue was modeled as glutamate. However, this high-resolution structure clearly identifies this residue as an arginine.

Residues 1−3 and 580−609 are not visible in the electron density maps. This is also the case in all other known *Curvularia* VCPO crystal structures with slightly varying lengths of the missing N−- and C-terminal parts. As natural and recombinant materials exhibit the same missing parts in the X-ray structure, a proteolytic cleavage of the enzyme before crystallization is very unlikely. No attempts were undertaken to determine the reason for the lack of these parts in the X-ray structures because these residues are far away from the essential portions of the enzyme structure.

Intermediate Trapped in the Active Site of Apo-VCPO-pNPP. In the initial difference electron density map for the recombinant apoenzyme, a strong electron density (greater than 4σ) was found at the active site (*2*). Because no vanadate was added to the recombinant protein before or during crystallization, it was assumed that the species bound to the metal cofactor-binding site could be a tetrahedral sulfate anion, present in high concentrations in the crystallization buffer. The presence of a number of positively charged residues, which usually form hydrogen bonds with the vanadate, probably stabilizes the strong negative charge of the sulfate ion. Thus, a tetrahedral sulfate was built into the difference electron density and refined. The final omit map for His496 and the sulfate group close by is displayed in Figure 1 and shows clearly the density for the bound oxyanion. Figure 1 shows a scheme of the interactions between the sulfate and the active site residues. The sulfur atom is 2.92 Å away from the ϵ-nitrogen of the side chain of His496 and is held by hydrogen bonds to the side chains of Lys353 (2.81 Å), Arg490 (3.01 Å), Arg360 (3.01 Å), His404 (2.99 Å), and Ser402 (2.69 Å) and additionally to the main chain nitrogen atoms of Gly403 (2.80 Å) and His404 (3.21 Å) and to a water molecule (2.53 Å). His496 is positioned by a strong hydrogen bond to the side chain of Asp500 (2.93 Å) (see also Table 2).

Since crystals that diffracted as well could be obtained with ammonium sulfate as a precipitant only, the reaction of apo-VCPO with pNPP had to be performed in the presence of sulfate in the mother solution. This sulfate ion may in fact interfere with the binding of pNPP to the active site and obscure the results and interpretation. However, the inhibition of VCPO by sulfate is very weak, whereas the affinity for pNPP is very high (reported K_m value for pNPP $\ll$ 50 μM (*2*, *5*)). In our setup (1 mM pNPP), the expected occupancy of the active site by sulfate is low.

The initial electron density map for the apo-VCPO-pNPP complex structure was calculated by omitting the vanadate ligand His496 and the sulfate molecule present in the active site of the apo-VCPO crystal structure. The difference

Table 2: Hydrogen-Bonding Pattern around the Active Site of Apo-VCPO-pNPP, Apo-SO_4-VCPO, and PhoN (PDB ID 3BB0, 1VNS, and 2A96, Respectively)

atom X	atom Y	distance (Å)
Gly403 N	PO_3 O4	2.76
	SO_4 O2	2.80
Gly157 N	PO_4 O4	2.90
His404 N	PO_3 O3	3.12
	SO_4 O4	3.19
His158 N	PO_4 O1	2.71
Lys353 N^{ζ}	PO_3 O4	2.69
	SO_4 O2	2.81
Lys123 N^{ζ}	PO_4 O4	2.59
Arg360 $N^{\eta 2}$	PO_3 O4	3.66
	SO_4 O2	3.38
Arg130 $N^{\eta 2}$	PO_4 O4	3.5
Arg360 $N^{\eta 1}$	PO_3 O2	3.05
	SO_4 O1	3.01
Arg130 $N^{\eta 1}$	PO_4 O2	3.04
Ser402 O^{γ}	PO_3 O3	2.59
	SO_4 O4	2.69
Ser156 O^{γ}	PO_4 O1	2.94
Arg490 N^{ϵ}	PO_3 O3	3.08
	SO_4 O4	3.20
Arg191 N^{ϵ}	PO_4 O1	3.90
Arg490 $N^{\eta 2}$	PO_3 O2	2.85
	SO_4 O1	3.01
Arg490 $N^{\eta 2}$	PO_3 O2	3.40
His496 $N^{\epsilon 2}$	PO_3 P1	2.14
	SO_4 S	2.92
His197 $N^{\epsilon 2}$	PO_4 P	2.90
HOH801A O	PO_3 P1	3.06
HOH801B O	PO_3 P1	4.56
1111 O	SO_4 S	2.53
HOH1139 O	HOH801A	3.07
His404 $N^{\delta 1}$	HOH801A	2.80
	SO_4 O3	2.99
His158 $N^{\delta 1}$	PO_4 O1	2.96
	PO_4 O3	3.03
HOH1139 O	HOH801B	2.97
HOH1139 O	Asp292 $O^{\delta 1}$	2.87
Arg490 $N^{\eta 2}$	Asp292 $O^{\delta 1}$	2.86
	Asp292 $O^{\delta 1}$	2.89
Arg191 $N^{\eta 2}$	no counterpart	
Arg490 $N^{\eta 1}$	Asp292 $O^{\delta 2}$	2.91
	Asp292 $O^{\delta 2}$	2.98
Arg191 $N^{\eta 1}$	no counterpart	
His496 $N^{\delta 1}$	Asp500 $O^{\delta 2}$	2.68
	Asp500 $O^{\delta 2}$	2.95
His197 $N^{\delta 1}$	Asp202 $O^{\delta 2}$	3.28

electron density map contoured at 4.0σ is displayed in Figure 2. It shows electron density for the His496 residue and a planar density with C_3 symmetry with a continuous density to the His496 residue. This electron density has been modeled as metaphosphate anion PO_3^- bound with its phosphorus atom to the ϵ-nitrogen atom of His496. Since a sulfur bond with a nitrogen of a histidine has never been reported before, it is highly unlikely that the continuous density is due to residual sulfate forming a SN bond with the nitrogen of His496. The discrete electron density on top of the PO_3^- group has been assigned to two disordered water molecules, whose occupancies have been determined to be 0.63 for the lower situated water molecule and 0.37 for the upper one. The active site without the electron density is shown in Figure 3. Here, the hydrogen-bonding pattern around the active site is included, whereby the actual hydrogen-bond distances are listed in Table 2. This pattern is very similar to that found in the sulfate-bound apo-VCPO structure. The difference is that the sulfate group is further away from the His496 side chain, forming no covalent bond between the sulfur atom of the sulfate and the $N^{\epsilon 2}$ atom of His496 and the absence of the water molecule HOH801A. In apo-VCPO-pNPP, the distance between the phosphorus atom P1 of the PO_3^- group to the $N^{\epsilon 2}$ atom of His496 is 2.14 Å only and corresponds to a covalent bond between these two groups. For comparison, the noncovalent interatomic distance between the phosphorus atom of the bound phosphate and His197 in PhoN is 2.8 Å (*14*). The apical water molecule HOH801A is within hydrogen-bonding distance to PO_3^- P1 and is in a perfect position for a nucleophilic attack of the metaphosphate−histidine intermediate to form the inorganic phosphate. The characterized reaction intermediate corresponds to state E in the mechanistic scheme for the hydrolysis of a phosphate monoester by apo-VCPO proposed by Renirie et al. (*5*) (see Figure 4). An attacking water in the same position has also been proposed in the reaction scheme given by Makde et al. (*14*) for PhoN.

The reaction intermediate deserves a special consideration. Phosphoryl transfer reactions have been intensively studied, and the current state of knowledge has been pointed out in a recent article (*24*). The occasion for this commentary was the characterization of an intermediate formed in the phosphoryl transfer from C(1)O of glucose-(bis)phosphate to the nucleophilic Asp8 carboxylate in the atomic resolution structure of phosphorylated β-phosphoglucomutase (*25*). The geometry of the intermediate is comparable to that of

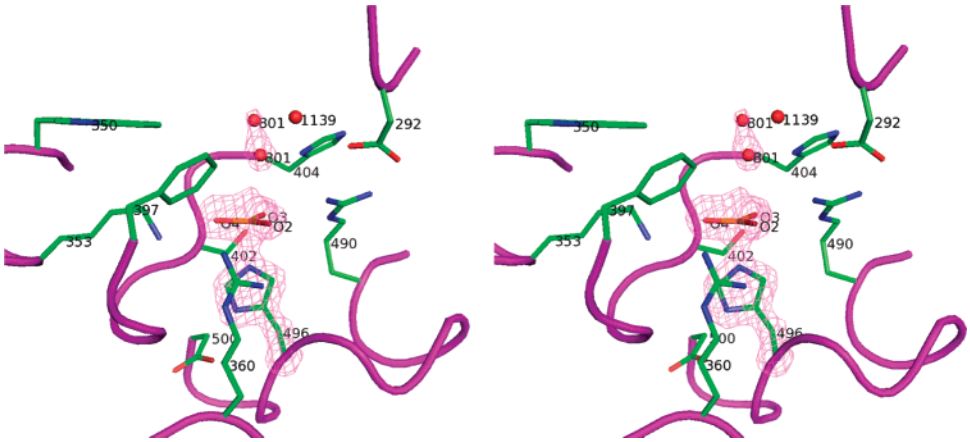

FIGURE 2: Stereoview of the model of the active site of the apo-VCPO-pNPP crystal structure. The electron density map contoured at 4.0σ was calculated after omitting His496 and the bound metaphosphate ion.

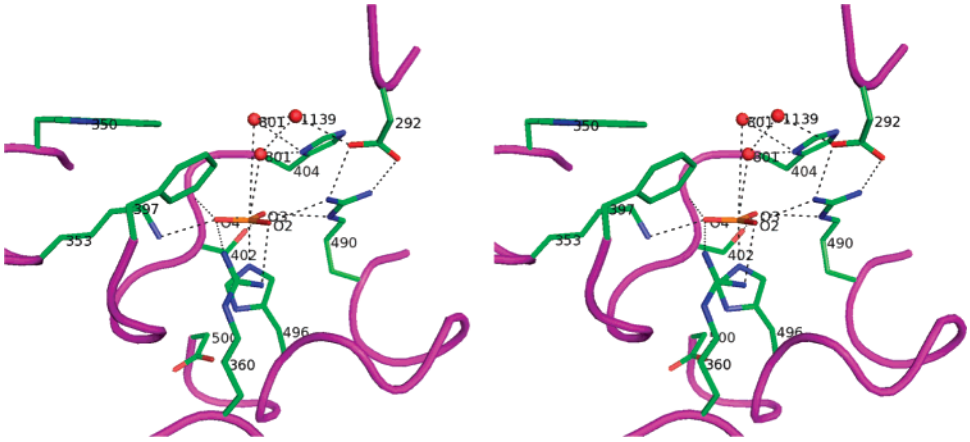

FIGURE 3: Stereoview of the hydrogen-bonding pattern around the active site of the apo-VCPO-pNPP crystal structure. The hydrogen bonds and other interactions with the metaphosphate ion are represented as dashed lines, and the distances are given in Table 2 or in the text.

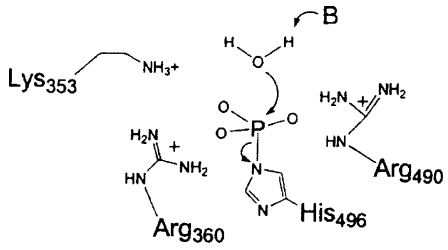

FIGURE 4: Schematic drawing of state E in the mechanistic scheme for the hydrolysis of a phosphate monoester by apo-VCPO proposed by Renirie et al. (*5*).

pentavalent oxyphosphoranes with equatorial bond lengths of 1.57−1.63 Å and apical phosphorus−oxygen bond lengths of 1.66−1.76 Å. This intermediate would correspond to the complex between the substrate and the enzyme cleaving off the alcoholic product. The intermediate characterized in this crystal structure is different than that of β-phosphoglucomutase in two aspects. First, the active site residue is a histidine with an apical nitrogen coordinating atom, and second, this intermediate is the step before the phosphate is released.

The P−N distance has been determined to about 2.1 Å. This bond length is somewhat greater than that found in phosphonoimidazolidine compounds. In the crystal structure of 1-carboxymethyl-2-imino-3-phosphonoimidazolidine, the P−N distance is, for example, 1.74 Å (*26*). However, the PO_3^- group is nearly planar in the pNPP−VCPO structure. This means that the P atom moves away from the N atom, thus increasing the bond distance and decreasing the strength of this bond. This will be caused by the attacking water molecule, which is already in a distance of about 3.0 Å to the P atom.

Comparison of the Active Sites of PhoN and Apo-VCPO. Figure 5 shows the overlay of the active sites, and Table 2 contains the detailed bond and hydrogen-bond structure for both proteins. It is evident from these two resources that the active sites are similar to a great extent but that there are also several striking differences, which are located in the upper part of Figure 5. Asp292 of apo-VCPO has no counterpart in the PhoN structure, and therefore, no salt bridge can be formed by the respective Arg191. The two putative halide binding residues Trp350 and Phe397 in VCPO are bulky and hydrophobic as compared to corresponding alanine and aspartate in PhoN. This makes the active site more accessible in PhoN as in apo-VCPO, and the aspartate residue creates a negative electrostatic potential in the relevant surface area. Despite the high affinity of apo-VCPO for pNPP ($K_m \ll 50$ μM) (*5*), it is clear from the reported turnover values that VCPO is optimized for haloperoxidase activity; $k_{cat} = 20$ s^{-1} for Cl^- oxidation and 120 s^{-1} for Br^- oxidation (*1*) versus 1.2 min^{-1} for pNPP hydrolysis (*5*). The presence of Trp350 and Phe397 may

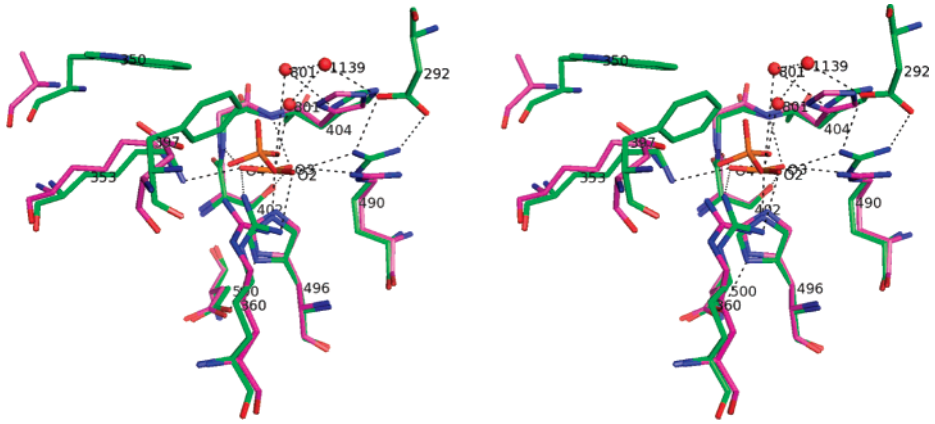

FIGURE 5: Stereoview of the overlay of the active sites of apo-VCPO-pNPP and PhoN. Bonds and hydrogen bonds are included as dashed lines for apo-VCPO-pNPP only. The actual bond distances for both structures and the residue numbers for the homologous residues of PhoN are given in Table 2. The color code for carbon atoms is green for apo-VCPO-pNPP and pink for PhoN.

partially explain the low phosphatase activity of apo-VCPO. Further mutagenesis studies may shed light on this issue.

CONCLUSION

This high-resolution crystal structure of the reaction of the phosphate monoester pNPP with apo-VCPO exhibits a trapped intermediate of the phosphohydrolase reaction. The intermediate consists of metaphosphate anion PO_3^- covalently bound via its phosphorus atom to the $N^{\epsilon 2}$ atom of the protein ligand His496. An apical water molecule is ready for a nucleophilic attack of the metaphosphate−histidine intermediate to form the inorganic phosphate, which is then released. This is, to our knowledge, the first structural characterization of a real reaction intermediate of the inorganic phosphate group release in a dephosphorylation reaction. All other complex structures were obtained with transition-state analogues such as vanadate, tungstate, molybdate, and sulfate.

REFERENCES

1. Hemrika, W., Renirie, R., Macedo-Ribeiro, S., Messerschmidt, A., and Wever, R. (1999) Heterologous expression of the vanadium-containing chloroperoxidase from *Curvularia inaequalis* in *Saccharomyces cerevisiae* and site-directed mutagenesis of the active site residues His(496), Lys(353), Arg(360), and Arg(490), *J. Biol. Chem. 274*, 23820−23827.
2. Macedo-Ribeiro, S., Hemrika, W., Renirie, R., Wever, R., and Messerschmidt, A. (1999) X-ray crystal structures of active site mutants of the vanadium-containing chloroperoxidase from the fungus *Curvularia inaequalis*, *J. Biol. Inorg. Chem. 4*, 209−219.
3. Messerschmidt, A., Prade, L., and Wever, R. (1997) Implications for the catalytic mechanism of the vanadium-containing enzyme chloroperoxidase from the fungus *Curvularia inaequalis* by X-ray structures of the native and peroxide form, *Biol. Chem. 378*, 309−315.
4. Messerschmidt, A., and Wever, R. (1996) X-ray structure of a vanadium-containing enzyme: Chloroperoxidase from the fungus *Curvularia inaequalis*, *Proc. Natl. Acad. Sci. U.S.A. 93*, 392−396.
5. Renirie, R., Hemrika, W., and Wever, R. (2000) Peroxidase and phosphatase activity of active-site mutants of vanadium chloroperoxidase from the fungus *Curvularia inaequalis*. Implications for the catalytic mechanisms, *J. Biol. Chem. 275*, 11650−11657.
6. Isupov, M. N., Dalby, A. R., Brindley, A. A., Izumi, Y., Tanabe, T., Murshudov, G. N., and Littlechild, J. A. (2000) Crystal structure of dodecameric vanadium-dependent bromoperoxidase from the red algae *Corallina officinalis*, *J. Mol. Biol. 299*, 1035−1049.
7. Weyand, M., Hecht, H., Kiess, M., Liaud, M., Vilter, H., and Schomburg, D. (1999) X-ray structure determination of a vanadium-dependent haloperoxidase from *Ascophyllum nodosum* at 2.0 Å resolution, *J. Mol. Biol. 293*, 595−611.
8. Hemrika, W., Renirie, R., Dekker, H. L., Barnett, P., and Wever, R. (1997) From phosphatases to vanadium peroxidases: A similar architecture of the active site, *Proc. Natl. Acad. Sci. U.S.A. 94*, 2145−2149.
9. Neuwald, A. F. (1997) An unexpected structural relationship between integral membrane phosphatases and soluble haloperoxidases, *Protein Sci. 6*, 1764−1767.
10. Stukey, J., and Carman, G. M. (1997) Identification of a novel phosphatase sequence motif, *Protein Sci. 6*, 469−472.
11. Brindley, D. N., and Waggoner, D. W. (1998) Mammalian lipid phosphate phosphohydrolases, *J. Biol. Chem. 273*, 24281−24284.
12. Tanaka, N., Hasan, Z., Hartog, A. F., van Herk, T., and Wever, R. (2003) Phosphorylation and dephosphorylation of polyhydroxy compounds by class A bacterial acid phosphatases, *Org. Biomol. Chem. 1*, 3470.
13. Ishikawa, K., Mihara, Y., Gondoh, K., Suzuki, E., and Asano, Y. (2000) X-ray structures of a novel acid phosphatase from *Escherichia blattae* and its complex with the transition-state analogue molybdate, *EMBO J. 19*, 2412−2423.
14. Makde, R. D., Mahajan, S. K., and Kumar, V. (2007) Structure and mutational analysis of the PhoN protein of *Salmonella typhimurium* provide insight into mechanistic details, *Biochemistry 46*, 2079−2090.
15. Littlechild, J., Garcia-Rodriguez, E., Dalby, A., and Isupov, M. (2002) Structural and functional comparisons between vanadium haloperoxidase and acid phosphatase enzymes, *J. Mol. Recognit. 15*, 291−296.
16. Leslie, A. G. (1999) Integration of macromolecular diffraction data, *Acta Crystallogr., Sect. D: Biol. Crystallogr. 55*, 1696−1702.
17. Collaborative Computational Project (1994) The CCP4 suite: Programs for protein crystallography, *Acta Crystallogr., Sect. D: Biol. Crystallogr. 50*, 760−763.
18. Murshudov, G. N., Vagin, A. A., and Dodson, E. J. (1997) Refinement of macromolecular structures by the maximum-likelihood method, *Acta Crystallogr., Sect. D: Biol. Crystallogr. 53*, 240−255.
19. Range, K., McGrath, M. J., Lopez, X., and York, D. M. (2004) The structure and stability of biological metaphosphate, phosphate, and phosphorane compounds in the gas phase and in solution, *J. Am. Chem. Soc. 126*, 1654−1665.
20. Laskowski, R. A., MacArthur, M. W., Moss, D. S., and Thornton, J. M. (1993) PROCHECK: A program to check the stereochemical quality of protein structures, *J. Appl. Crystallogr. 26*, 283−291.
21. Kleywegt, G. J., and Jones, T. A. (1994) A superposition, *ESRF/CCP4 Newsletter 31*, 9−14.
22. DeLano, W. L. (2003) *The PyMol Molecular Graphics System*, DeLano Scientific LLC, San Carlos, CA.
23. Simons, B. H., Barnett, P., Vollenbroek, E. G., Dekker, H. L., Muijsers, A. O., Messerschmidt, A., and Wever, R. (1995) Primary structure and characterization of the vanadium chloroperoxidase from the fungus *Curvularia inaequalis*, *Eur. J. Biochem. 229*, 566−574.
24. Knowles, J. (2003) Chemistry: seeing is believing, *Science (Washington, DC, U.S.) 299*, 2002−2003.
25. Lahiri, S. D., Zhang, G. F., Dunaway-Mariano, D., and Allen, K. N. (2003) The pentacovalent phosphorus intermediate of a phosphoryl transfer reaction, *Science (Washington, DC, U.S.) 299*, 2067−2071.
26. Phillips, G. N., Thomas, J. W., Annesley, T. M., and Quiocho, F. A. (1979) Stereospecificity of creatine kinase: Crystal structure of 1-carboxymethyl-2-imino-3-phosphonoimidazolidine, *J. Am. Chem. Soc. 101*, 7120−7121.

BI7018628